Human Molecular Genetics, 2014, Vol. 23, No. 6 **1413–1424**
doi:10.1093/hmg/ddt528
Advance Access published on October 23, 2013

Abnormal mitochondrial transport and morphology are common pathological denominators in SOD1 and TDP43 ALS mouse models

Jordi Magrané[1,*], Czrina Cortez[1], Wen-Biao Gan[2] and Giovanni Manfredi[1,*]

[1]Brain and Mind Research Institute, Weill Medical College of Cornell University, New York, NY 10065, USA and [2]Skirball Institute, Department of Physiology and Neuroscience, New York University School of Medicine, New York, NY 10016, USA

Received August 23, 2013; Revised and Accepted October 17, 2013

Neuronal mitochondrial morphology abnormalities occur in models of familial amyotrophic lateral sclerosis (ALS) associated with SOD1 and TDP43 mutations. These abnormalities have been linked to mitochondrial axonal transport defects, but the temporal and spatial relationship between mitochondrial morphology and transport alterations in these two distinct genetic forms of ALS has not been investigated *in vivo*. To address this question, we crossed SOD1 (wild-type $SOD1^{WT}$ and mutant $SOD1^{G93A}$) or TDP43 (mutant $TDP43^{A315T}$) transgenic mice with mice expressing the fluorescent protein Dendra targeted to mitochondria in neurons (mitoDendra). At different time points during the disease course, we studied mitochondrial transport in the intact sciatic nerve of living mice and analyzed axonal mitochondrial morphology at multiple sites, spanning from the spinal cord to the motor terminals. Defects of retrograde mitochondrial transport were detected at 45 days of age, before the onset of symptoms, in $SOD1^{G93A}$ and $TDP43^{A315T}$ mice, but not in $SOD1^{WT}$. At later disease stages, also anterograde mitochondrial transport was affected in both mutant mouse lines. In $SOD1^{G93A}$ mice, mitochondrial morphological abnormalities were apparent at 15 days of age, thus preceding transport abnormalities. Conversely, in $TDP43^{A315T}$ mice, morphological abnormalities appeared after the onset of transport defects. Taken together, these findings demonstrate that neuronal mitochondrial transport and morphology abnormalities occur *in vivo* and that they are common denominators of different genetic forms of the ALS. At the same time, differences in the temporal and spatial manifestation of mitochondrial abnormalities between the two mouse models of familial ALS imply that different molecular mechanisms may be involved.

INTRODUCTION

Numerous lines of evidence indicate that mitochondrial dysfunction is involved in amyotrophic lateral sclerosis (ALS). Biochemical and morphological mitochondrial abnormalities have been observed in patients affected by sporadic ALS or familial ALS (FALS), as well as in cell culture and animal models of FALS (reviewed in 1,2). In transgenic mouse models of FALS associated with mutant SOD1 (3), mitochondrial dysfunction and abnormal mitochondrial morphology in the nervous system arise early on in the course of the disease (4–10), suggesting that these alterations may be predisposing motor neurons to degenerate. Furthermore, in mutant TDP43 transgenic mice, abnormal clustering of mitochondria has been described in the cell bodies of spinal cord motor neurons (11,12). Mutant or wild-type TDP43 overexpression in cultured motor neurons induced mitochondrial morphology and transport abnormalities, similar to those found in mutant SOD1 mice (13), although such abnormalities have not been examined *in vivo*.

Mitochondrial transport and morphology defects in ALS motor neurons were first demonstrated in cultured primary neurons (14–17). However, the *ex vivo* systems have several intrinsic limitations. First, the embryonic neurons investigated may not be fully representative of the adult disease conditions.

*To whom correspondence should be addressed at: Brain and Mind Research Institute, Weill Medical College of Cornell University, 407 East 61st St., New York, NY 10065, USA. Tel: +1 6469628174 (J.M.); 6469628172 (G.M.); Fax: +1 6469620535. Email: jom2005@med.cornell.edu (J.M.); gim 2004@med.cornell.edu (G.M.)

© The Author 2013. Published by Oxford University Press. All rights reserved.
For Permissions, please email: journals.permissions@oup.com

Second, the fundamental effects of the tissue environment, which are especially relevant in non-cell autonomous diseases, such as ALS (18), cannot be fully assessed using purified motor neuron cultures. And third, the energy requirements of the different regions of the motor neurons are likely to be very different *in vivo* than in the culture dish, where the environment is artificially controlled. Recent work has shown mitochondrial transport (19,20) or mitochondrial morphological changes (10) in the motor axons of mutant SOD1 mice. Here, we performed an *in vivo* comparative correlation between the changes in mitochondrial transport and morphology, in two distinct mouse models of FALS, SOD1 and TDP43 mutants.

Using high-resolution *in vivo* imaging, we studied mitochondrial transport and morphology in the intact sciatic nerves of FALS mouse models at different time points during disease course; we also analyzed mitochondrial morphology and distribution in proximal and terminal segments of motor axons and at the neuromuscular junction (NMJ). To take on these spatio-temporal studies, we crossed SOD1 ($SOD1^{WT}$, $SOD1^{G93A}$) and $TDP43^{A315T}$ mice to a new transgenic mouse expressing a fluorescent protein targeted to mitochondria (mitoDendra) in neurons.

Our data demonstrated that axonal mitochondrial transport was affected early on in the disease, before the onset of symptoms, in the sciatic nerves of both FALS mice. Therefore, mitochondrial abnormalities in neurons not only occur *in vivo* but they are also common pathological denominators in FALS and may participate to disease pathogenesis. Although SOD1 and TDP43 mutant mice shared several features of mitochondrial transport and morphology alterations, which were not observed in $SOD1^{WT}$ mice and mitoDendra controls, they differed in the temporal and spatial characteristics of these abnormalities, suggesting that the underlying mechanisms may vary in the different genetic forms of ALS.

RESULTS

MitoDendra-FALS double transgenic mice

To study mitochondrial morphology and dynamics in the nervous system *in vivo*, we generated a transgenic mouse with targeted expression of Dendra fluorescent protein to mitochondria (mitoDendra), under the control of the neuronal-specific Thy1.2 promoter (21). MitoDendra allows for direct imaging of mitochondria in living neurons (16).

The mitoDendra line, generated and maintained in the B6SJLF1 background, was crossed with the $SOD1^{WT}$ and $SOD1^{G93A}$ mice, in the same genetic background. The double transgenic mitoDendra-$SOD1^{G93A}$ mice had an average age of onset (hindlimb clasping) at 106.7 days ($\pm$ 17.3 days, $n = 14$ mice) and an average survival of 140.7 days ($\pm$ 16.2 days, $n = 18$). The double transgenic mitoDendra-$SOD1^{WT}$ did not display any disease phenotype up to 2 years of age.

$TDP43^{A315T}$ mice were backcrossed to get a congenic B6SJLF1 line. The double transgenic mitoDendra-$TDP43^{A315T}$ mice presented the symptoms originally described in the $TDP43^{A315T}$ parental mice, which were in a mixed C57Bl6xCBA background (22). While in the published report, the average ages at disease onset and survival were 120 days and 155 days, respectively (22), in the mitoDendra-$TDP43^{A315T}$ mice disease in the B6SJLF1 background onset occurred at 126.9 $\pm$ 30.4 days ($n = 20$ mice) and survival at 205.2 $\pm$ 72.3 days ($n = 32$). The cause of death was neurogenic intestinal occlusion, followed by necrosis, as described previously (23).

Mitochondrial axonal transport abnormalities in FALS mice

We investigated mitochondrial axonal transport in the surgically exposed, intact, sciatic nerve of living mitoDendra-FALS mice and mitoDendra littermate controls, at different time points (15, 45 and 90 days of age). Mitochondrial movements were visually tracked for the duration of the live recording (a representative example is shown in Supplementary Material, Movie S1) in consecutive frames captured every 5 s, as shown in Figure 1A. We assessed the frequency of mitochondrial movement (i.e. the percentage of mobile mitochondria) in each direction (i.e. anterograde or retrograde), in the sciatic nerve axons for the time frame of the experiment (6 min). At 45 days of age, 22.5 $\pm$ 5.1% of axonal mitochondria were mobile ($n = 39$ axons, data not shown), similar to primary motor neuron cultures (16), and slightly higher than in nerve-muscle explants (24).

In $SOD1^{G93A}$ or $SOD1^{WT}$ mice at 15 days of age, there was no evidence of mitochondrial transport impairment, compared with mitoDendra littermate controls (data not shown). However, at 45 days of age, there was a significant reduction in the frequency of mitochondrial movement in $SOD1^{G93A}$ mice (Fig. 1B) compared with mitoDendra littermate controls (representative examples shown in Supplementary Material, Movies S1 and S2). Mitochondrial motility was further reduced at 90 days (Fig. 1B). When direction of movement was analyzed, we found a decrease in the proportion of retrograde moving mitochondria in $SOD1^{G93A}$ mice at 45 days (Fig. 1C); no significant differences were detected in the anterograde transport. By day 90, when $SOD1^{G93A}$ mice approached the symptomatic disease stage, the proportion of moving mitochondria was significantly reduced in both anterograde and retrograde directions (Fig. 1D). The proportion of moving mitochondria was unaffected in $SOD1^{WT}$ mice, at both 45 and 90 days of age (Fig. 1C and D).

Mitochondrial movement showed a trend toward a decrease in $TDP43^{A315T}$ mice at 45 days of age, compared with littermate controls (representative example shown in Supplementary Material, Movie S3), although this decrease did not reach statistical significance ($P = 0.056$ by Student's *t*-test; Fig. 1B). However, at 90 days, the frequency of mitochondrial movement was significantly reduced (Fig. 1B). The proportion of retrograde moving mitochondria was also significantly reduced at 45 days of age, when compared with controls (Fig. 1E). Similar to $SOD1^{G93A}$ mice, $TDP43^{A315T}$ mice at 90 days of age displayed a decrease in both anterograde and retrograde mitochondrial transport (Fig. 1F).

Together, these results indicate that neuronal mitochondrial transport is progressively affected in all ALS mouse models tested and that retrograde transport is affected earlier than anterograde transport.

Mitochondrial morphology and clustering abnormalities in the sciatic nerve of FALS mice

To investigate how transport abnormalities correlated with abnormal mitochondrial morphology and distribution in neurons,

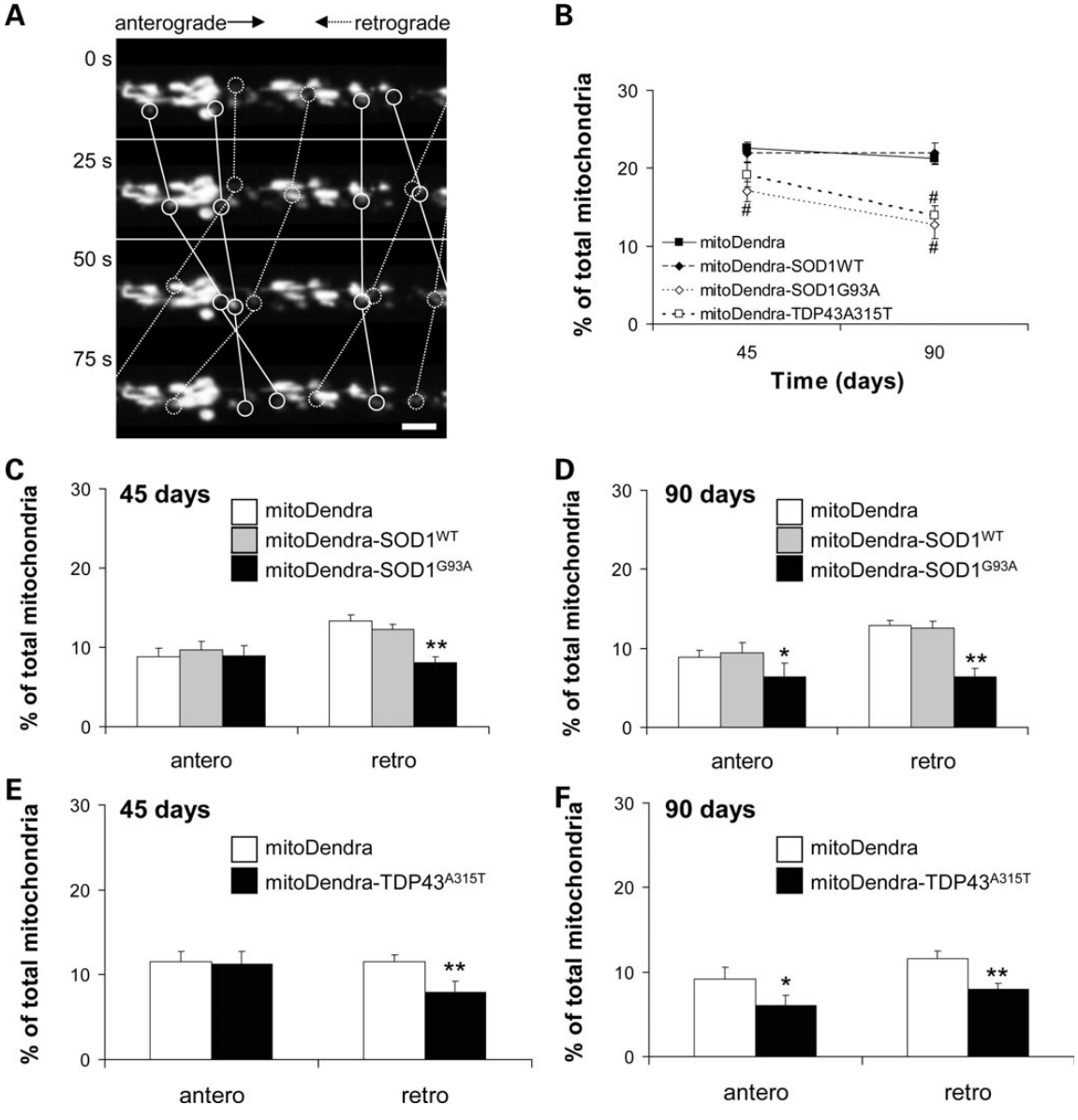

Figure 1. Retrograde transport of mitochondria is first altered in the sciatic nerves of mitoDendra-ALS mice. (**A**) Time-lapse microscopy of mitoDendra-labeled mitochondria in the intact sciatic nerve of a 45 days old mitoDendra mouse. Frames were acquired every 5 s for a total recording time of 6 min (the panels show some selected frames at 25 s intervals). Anterograde and retrograde mobile mitochondria are identified by solid lines (moving to the right of the panel) and dotted lines (moving to the left), respectively. Note that mitochondria are not always clearly visible in all the selected frames, because of the uneven course of the axon in the nerve, which crosses the focal planes several times. For representative movies from mitoDendra, mitoDendra-SOD1^{G93A} and mitoDendra-TDP43^{A315T} mice, see Supplementary Material, Movie S1, S2 and S3. Scale bar, 5 μm. (**B**) Analysis of mitochondrial transport in mitoDendra-ALS mice over time. *n* (axons at 45–90 days in 3–4 mice per group) = 39–46 mitoDendra, 22–26 mitoDendra-SOD1^{WT}, 35–22 mitoDendra-SOD1^{G93A} and 21–24 mitoDendra-TDP43^{A315T}. $^{\#}P < 0.01$ by Student's *t*-test, versus mitoDendra littermate controls. (**C**) Analysis of the direction of mitochondrial transport in mitoDendra-SOD1 mice at 45 days. *n* (axons in 3 mice per group) = 21 mitoDendra, 22 mitoDendra-SOD1^{WT} and 35 mitoDendra-SOD1^{G93A}. (**D**) Analysis of the direction of mitochondrial transport in mitoDendra-SOD1 mice at 90 days. *n* (axons in 3–4 mice per group) = 26 mitoDendra, 26 mitoDendra-SOD1^{WT} and 22 mitoDendra-SOD1^{G93A}. (**E**) Analysis of the direction of mitochondrial transport in mitoDendra-TDP43^{A315T} mice at 45 days. *n* (axons in 3 mice per group) = 18 mitoDendra, 21 mitoDendra-TDP43^{A315T}. (**F**) Analysis of the direction of mitochondrial transport in mitoDendra-TDP43^{A315T} mice at 90 days. *n* (axons in 4–5 mice per group) = 20 mitoDendra, 24 mitoDendra-TDP43^{A315T}. $^{*}P < 0.05$ and $^{**}P < 0.01$ by Student's *t*-test, versus mitoDendra controls. Error bars represent the SEM.

we analyzed sciatic nerves of mitoDendra-FALS mice at different time points (Fig. 2A).

The average length of mitochondria in the sciatic nerve of SOD1^{G93A} mice, but not of SOD1^{WT} mice, was decreased at 15 days of age, relative to mitoDendra controls (Fig. 2B). By 45 days of age, there was a further reduction in mitochondrial length in SOD1^{G93A} mice. The size reduction became even more pronounced by 90 days of age in SOD1^{G93A} mice (Fig. 2B), suggesting a progressive pathological phenotype that worsened in parallel to transport abnormalities. No mitochondrial length abnormalities were detected in the sciatic nerves of TDP43^{A315T} mice at 45 days of age (Fig. 2C),

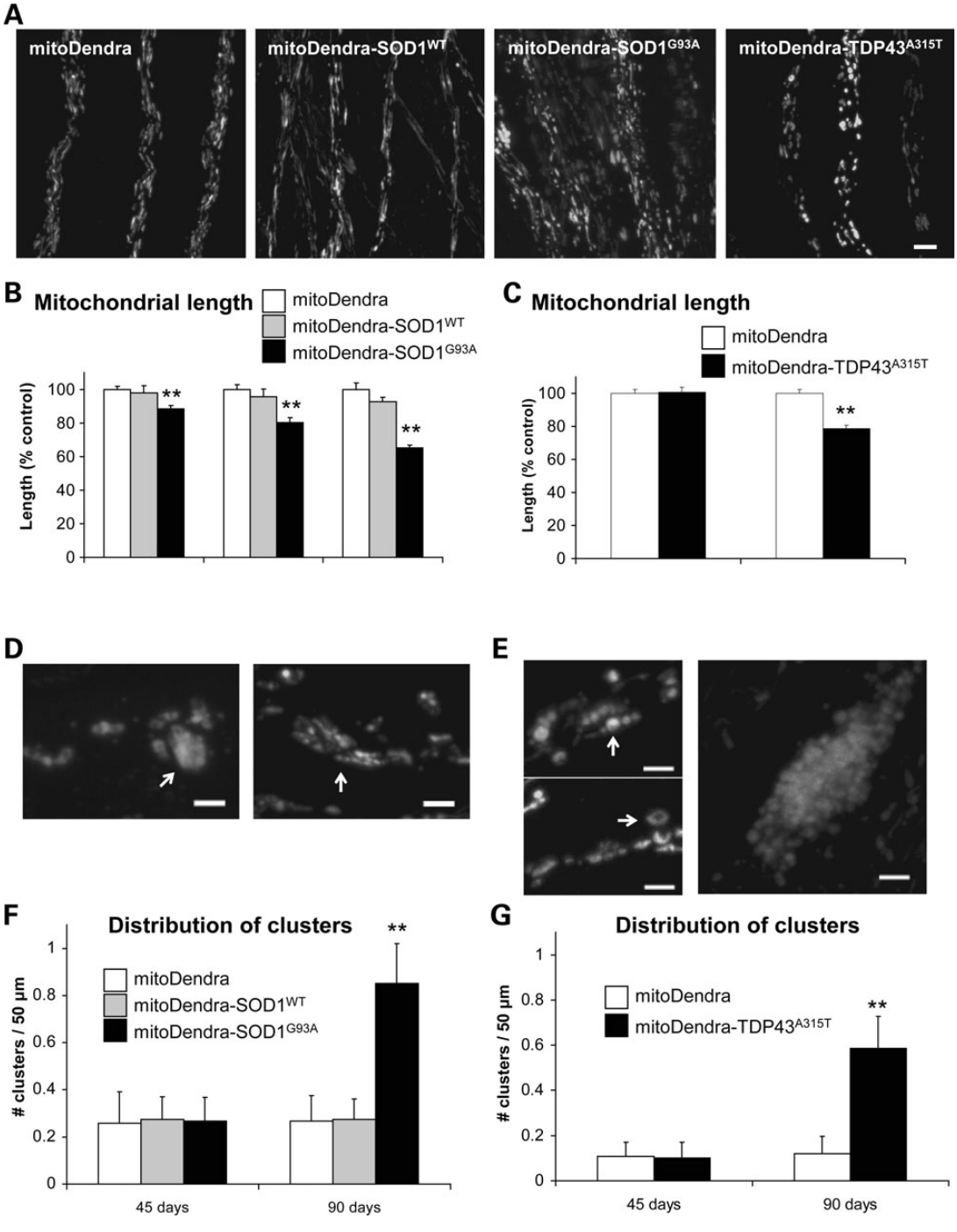

Figure 2. Mitochondria morphology abnormalities precede transport alterations in the sciatic nerves of mitoDendra-SOD1^{G93A} mice, but appear later in mitoDendra-TDP43^{A315T} mice. (**A**) Representative fields of several mitoDendra-labeled axons from the sciatic nerves of 90 days old FALS mice. Scale bar, 5 μm. (**B**) Quantification of the length of mitochondria in mitoDendra-SOD1 mice during disease progression. *n* (axons at 15–45–90 days in 3–4 mice per group) = 36–34–38 mitoDendra, 38–39–35 mitoDendra-SOD1^{WT}, 37–27–34 mitoDendra-SOD1^{G93A}. (**C**) Quantification of the length of mitochondria in mitoDendra-TDP43^{A315T} mice. *n* (axons at 45–90 days in 3–4 mice per group) = 26–41 mitoDendra and 31–37 mitoDendra-TDP43^{A315T}. (**D**) Details of morphologically abnormal, swollen mitochondria (left, arrow) and abnormal clustering (right, arrow) in the sciatic nerve of a 90 days old mitoDendra-SOD1^{G93A} mouse. Scale bar, 2 μm. (**E**) Details of beads-on-string structures (left, top, arrow) and doughnut mitochondria (left, bottom, arrow), and a cluster of mitochondria (right, arrow) in the sciatic nerve of a 90 days old mitoDendra-TDP43^{A315T} mouse. Scale bar, 2 μm. (**F**) Quantification of the frequency of clusters of mitochondria in the sciatic nerves during disease progression. *n* (axons at 45–90 days in 3 mice per group) = 24–32 mitoDendra, 33–40 mitoDendra-SOD1^{WT} and 28–29 mitoDendra-SOD1^{G93A}. (**G**) Quantification of the distribution of clusters of mitochondria in segments of the nerve during disease progression. *n* (axons at 45–90 days in 3–4 mice per group) = 27–41 mitoDendra, 31–40 mitoDendra-TDP43^{A315T}. In all panels, $^{**}P < 0.01$ by Student's *t*-test, versus mitoDendra controls. Error bars represent the SEM. In (B) and (C), values are expressed as mean percentage ± SEM of mitoDendra controls.

despite transport defects being already apparent (Fig. 1E). However, mitochondrial length was significantly reduced at 90 days of age (Fig. 2C).

In both $SOD1^{G93A}$ and $TDP43^{A315T}$, but not $SOD1^{WT}$ or controls, we observed the presence of mitochondrial clustering and abnormal looking mitochondria, along the sciatic nerve axons (Fig. 2D and E). Both clusters and abnormal mitochondria, however, showed distinct features of structure and appearance in $SOD1^{G93A}$ and $TDP43^{A315T}$ mice. Swollen mitochondria were identified in $SOD1^{G93A}$ (Fig. 2D, left panel), whereas mitochondria 'doughnuts' and rounded mitochondria tightly associated in beads-on-string structures were observed in $TDP43^{A315T}$ (Fig. 2E, left panels). In $SOD1^{G93A}$, we observed clustering of otherwise normal looking mitochondria (Fig. 2D, right panel), whereas in $TDP43^{A315T}$ mitochondria were massively accumulating in grape-like structures (Fig. 2E, right panel). When measured as number of axonal segments in which abnormal mitochondrial clustering was observed, these abnormalities were only significantly increased in FALS mice at 90 days of age, but not at 45 days (Fig. 2F and G).

These results, together with the data of mitochondrial transport, indicate that the sequence of events involving mitochondrial abnormalities *in vivo* is different in the sciatic nerves of $SOD1^{G93A}$ and $TDP43^{A315T}$ at early disease stages. In $TDP43^{A315T}$, defects in retrograde transport precede mitochondrial fragmentation and are followed by anterograde transport defects and mitochondrial abnormal clustering; in $SOD1^{G93A}$, the timing of the retrograde transport defects follows the early fragmentation of mitochondria. In both mouse models, the appearance of anterograde transport defects correlates with the presence of mitochondrial clusters at a more advanced disease stage.

Morphology defects in mobile mitochondria

Early mitochondrial morphology abnormalities in the sciatic nerve of $SOD1^{G93A}$ mice were followed by retrograde transport defects; however, mitochondrial morphology was affected in $TDP43^{A315T}$ mice only after the frequency of retrograde axonal transport was reduced. In order to gain insights into the relationship between motility and morphological abnormalities in these two FALS models, we determined the length of mobile mitochondria in the sciatic nerves of $SOD1^{G93A}$ and $TDP43^{A315T}$ mice at 45 days of age.

The length of both stationary and mobile mitochondria was significantly reduced in $SOD1^{G93A}$ mice, when compared with mitoDendra controls (Fig. 3A). Conversely, only mobile, and not stationary, mitochondria in $TDP43^{A315T}$ were significantly smaller than controls (Fig. 3B).

When lengths of mitochondria moving in the anterograde and retrograde directions were analyzed, we identified a reduction in the size of retrograde-moving mitochondria in the sciatic nerves of 45 days old $SOD1^{G93A}$ mice, but not in mitochondria moving in the anterograde direction (Fig. 3C). Interestingly, anterograde-moving mitochondria were significantly smaller in the sciatic nerves of $TDP43^{A315T}$ mice, while the difference did not reach statistical significance for retrograde-moving mitochondria ($P = 0.0938$ by Student's *t*-test; Fig. 3D), despite the lack of mitochondrial morphology abnormalities at 45 days (Fig. 2C).

These results indicate that in $SOD1^{G93A}$, but not in $TDP43^{A315T}$ mice, defects of retrograde mitochondrial transport correlate well with mitochondrial fragmentation and suggest that fragmented mitochondria in the sciatic nerve may originate in distal regions of the axon. The lack of similarities with $TDP43^{A315T}$ mice implies potential differences in the underlying molecular mechanisms of mitochondrial abnormalities in the two FALS models.

Mitochondrial morphology abnormalities are absent in the ventral roots of FALS mice

The sciatic nerve contains both motor and sensory axons, but only motor neurons are primary targets of the disease. In order to assess mitochondrial morphology abnormalities *in vivo* specifically in motor neurons, we analyzed the most proximal segments of the motor axons in the ventral roots of mitoDendra-FALS mice (Fig. 4A). At 90 days of age, when morphological and transport abnormalities are evident in the sciatic nerve, we did not observe changes in mitochondrial length or presence of clusters in the motor axons of $SOD1^{G93A}$ and $TDP43^{A315T}$ mice (Fig. 4B, bottom panels). Quantitative analysis of the length of mitochondria in the ventral roots of these mice demonstrated a lack of abnormalities in motor axons of both $SOD1^{G93A}$ (Fig. 4C) and $TDP43^{A315T}$ mice (Fig. 4D), compared with mitoDendra littermate controls.

We also analyzed the dorsal roots, which contain exclusively sensory neurons (Fig. 4A), which are not affected by the disease, in the same mice at 90 days of age. We observed neither morphological nor mitochondrial distribution changes in the FALS mice (Fig. 4B, top panels). As expected, quantitative analysis of mitochondrial morphology confirmed that there were no differences in the length of mitochondria in $SOD1^{G93A}$ (Fig. 4E) or $TDP43^{A315T}$ mice (Fig. 4F), when compared with controls.

Mitochondrial morphology and distribution alterations in the axon terminals and NMJs of FALS motor neurons

We then studied mitochondria in the most distal motor nerve segments, namely the nerve terminals and the NMJs, which degenerate early in the course of ALS (25,26). Although muscles from FALS mice show different degrees of paralysis, they all have a characteristic denervation phenotype (27). Neck muscles, such as trapezius, are similarly denervated as other disease relevant muscles, such as leg muscles (25,28). Flat muscles of the neck allow for easy detection of large numbers of NMJs. Therefore, we labeled motor axons and axon terminals from mitoDendra-FALS trapezius with antibodies against neurofilament 200 (NF200) and synaptophysin, while we identified NMJs by staining with fluorescent α-bungarotoxin (BTX) (Fig. 5A).

In the axonal terminals, we measured mitochondrial length and density (i.e. occupancy of mitochondria relative to the total area of the axonal segment). The average mitochondrial length was significantly reduced in motor terminals of $SOD1^{G93A}$ mice at 15 and 45 days of age, but not in $SOD1^{WT}$ and $TDP43^{A315T}$, in comparison with littermate controls (Fig. 5B and C). At 90 days of age, mitochondrial length was decreased in both $SOD1^{G93A}$ and $TDP43^{A315T}$ mice (Fig. 5B and C).

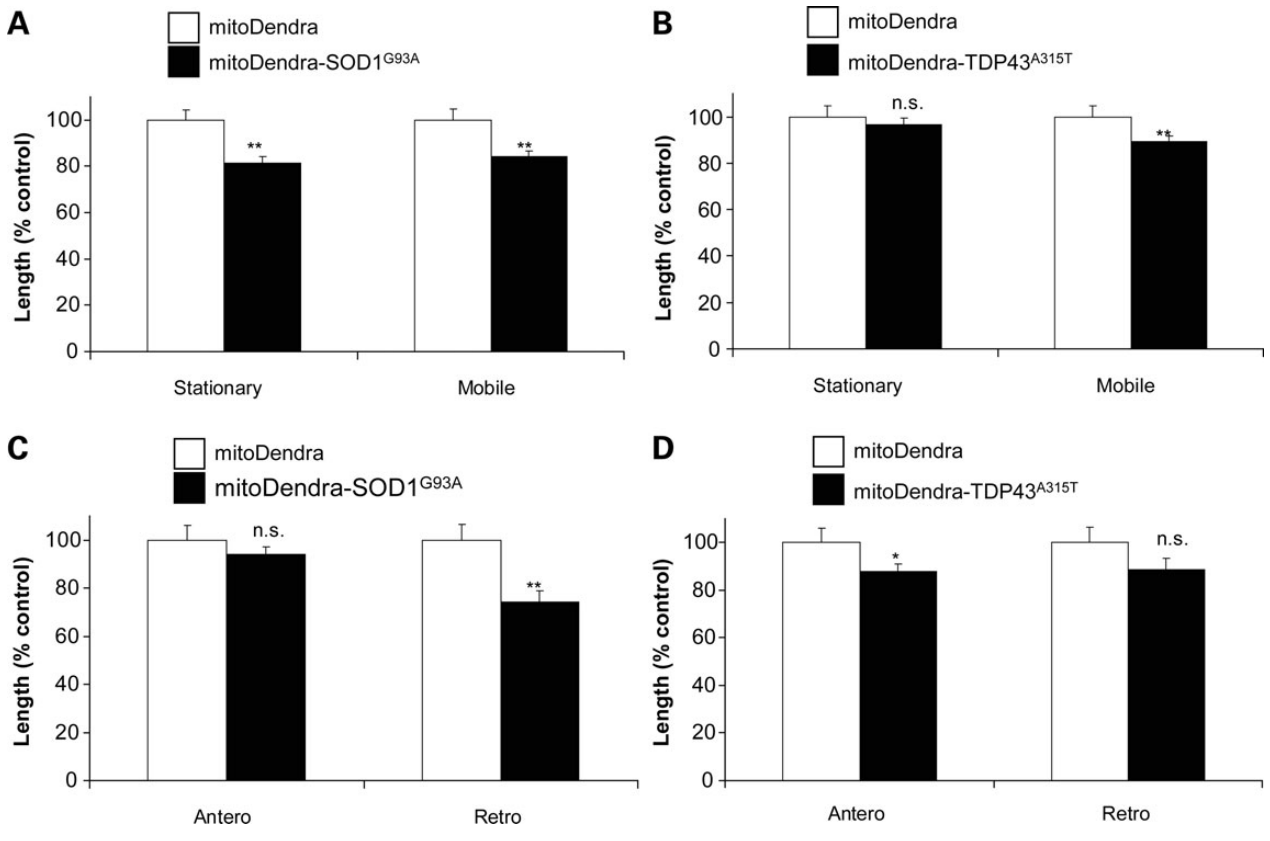

Figure 3. Abnormal mitochondria are transported in different directions in the sciatic nerves of mitoDendra-SOD1^{G93A} and mitoDendra-TDP43^{A315T} mice. (**A**) Correlation between length and movement of mitochondria in 45 days old mitoDendra-SOD1^{G93A} mice. *n* (axons in 3 mice per group) = 9 mitoDendra and 14 mitoDendra-SOD1^{G93A}. (**B**) Analysis of length and movement of mitochondria in 45 days old mitoDendra-TDP43^{A315T} mice. *n* (axons in 3 mice per group) = 8 mitoDendra and 9 mitoDendra-TDP43^{A315T}. (**C**) Correlation with the direction of mitochondrial transport in 45 days old mitoDendra-SOD1^{G93A} mice. (**D**) Correlation with the direction of mitochondrial transport in 45 days old mitoDendra-TDP43^{A315T} mice. $^{*}P < 0.05$ and $^{**}P < 0.01$ by Student's *t*-test, versus mitoDendra controls. n.s., non-significant. Error bars represent the SEM. Values are expressed as mean percentage ± SEM of mitoDendra controls.

No changes were observed in mitochondrial density at the motor axon terminals at 15 days of age, while there was a statistically significant decrease in SOD1^{G93A} mice at 45 and 90 days of age, when compared with controls (Fig. 5D), indicating that there was a depletion of mitochondria from the nerve terminal. On the other hand, mitochondrial density at the motor axon terminal was significantly increased in TDP43^{A315T} mice at 90 days of age (Fig. 5E), indicating an accumulation of mitochondria at the nerve terminals.

At the NMJs, where mitochondria are tightly packed and boundaries of individual organelles cannot be defined, we assessed mitochondrial density (i.e. % of occupancy of mitochondria over the total area of the NMJ; Fig. 5A). To focus on earlier events, preceding the complete degeneration of the NMJ, we analyzed motor terminals that ended into innervated NMJs, as previously defined (27). Mitochondrial density at the NMJ was significantly decreased in the SOD1^{G93A} mice by 90 days of age, but not at 45 days (Fig. 5F). There was no mitochondrial depletion at any time point analyzed in TDP43^{A315T} and SOD1^{WT} mice (Fig. 5F and G).

These results indicate that in SOD1^{G93A} mice, early fragmentation of mitochondria in the motor axon terminals is followed by a depletion of mitochondria in motor terminals and NMJs, by the time denervation becomes apparent (25). On the other hand, in TDP43^{A315T} mice, mitochondria appear normal but tend to accumulate in the distal portion of TDP43^{A315T} motor axons.

DISCUSSION

Previous work indicated that embryonic mutant SOD1 motor neurons in culture contained morphologically abnormal mitochondria and displayed altered axonal transport of mitochondria (16). Our work and others' have correlated these changes with the evidence that mutant SOD1 causes axonal shortening of cultured motor neurons (15,16,29,30). Undoubtedly, the *in vitro* system has value, because it allows for manipulations that are not feasible *in vivo*, but it also has intrinsic limitations. One crucial difference in studying neuronal mitochondrial dynamics *in vitro* and *in vivo* is the presence of myelination *in vivo*, which is likely to greatly affect mitochondrial distribution and motility, especially in the large axons of the major motor nerves (31). In addition, *in vivo* systems allow for the investigation of the progressive nature of mitochondrial transport abnormalities in longitudinal studies in their natural tissue context, where different cell types are represented, such as astroglia and microglia. Despite the advantages of the *in vivo* system, the investigation of mitochondrial changes in adult animal models of FALS has

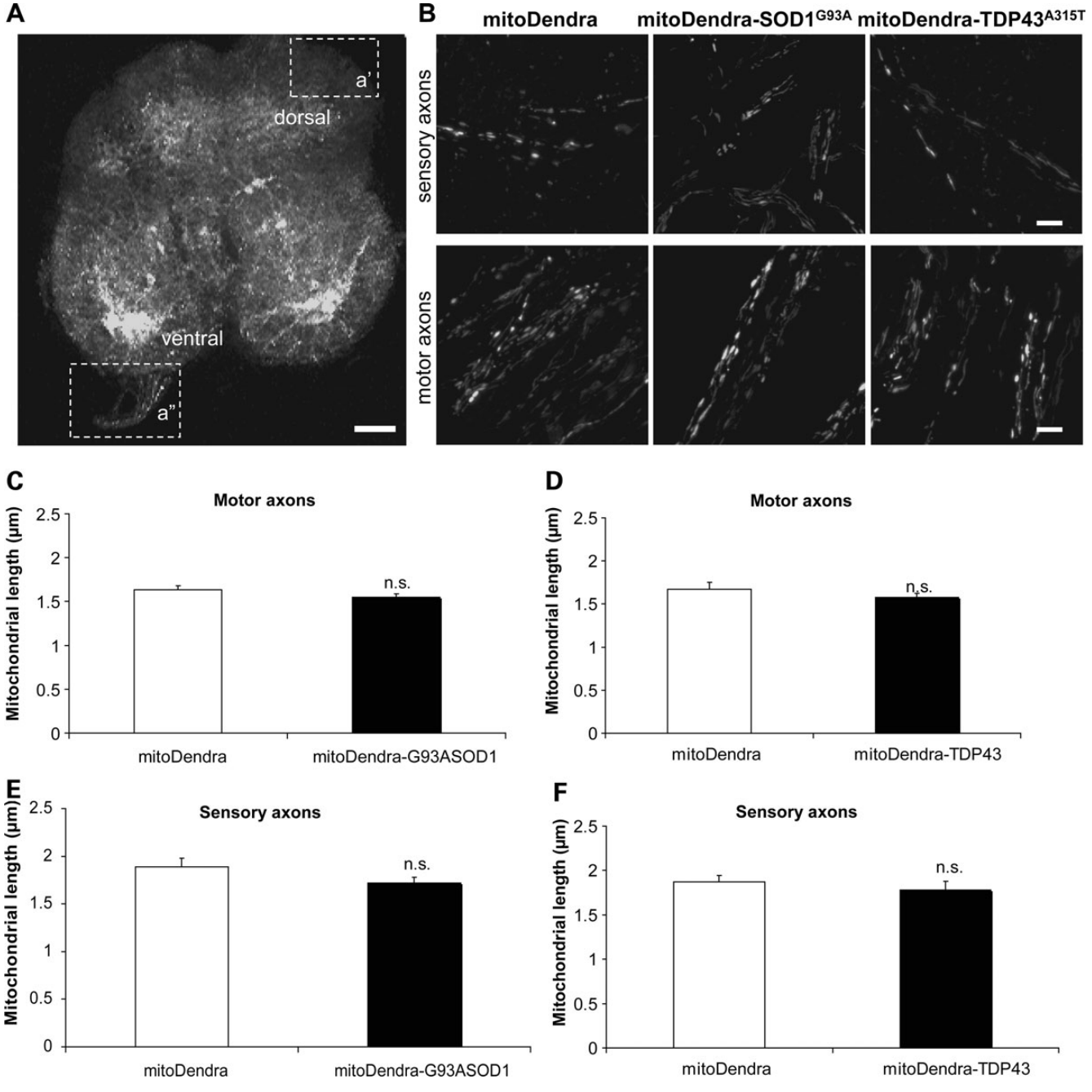

Figure 4. Lack of mitochondrial abnormalities in the proximal segments of motor and sensory axons. (**A**) Lumbar spinal cord section from a mitoDendra mouse. Mitochondrial lengths were measured from axons projecting from the ventral horn (motor axons, a″) and the dorsal horn (sensory axons, a′). Scale bar, 100 µm. (**B**) Representative images of motor and sensory axons from 90 days old mitoDendra, mitoDendra-SOD1^{G93A} and mitoDendra-TDP43^{A315T} mice. Scale bar, 5 µm. (**C**) Quantification of the length of mitochondria in motor axons of 90 days old mitoDendra-SOD1 mice. *n* (axons in 3 mice per group) = 26 mitoDendra and 17 mitoDendra-SOD1^{G93A}. (**D**) Quantification of the length of mitochondria in motor axons of 90 days old mitoDendra-TDP43^{A315T} mice. *n* (axons in 3 mice per group) = 20 mitoDendra and 29 mitoDendra-TDP43^{A315T}. (**E**) Quantification of the length of mitochondria in sensory axons of 90 days old mitoDendra-SOD1 mice. *n* (axons in 3 mice per group) = 15 mitoDendra and 12 mitoDendra-SOD1^{G93A}. (**F**) Quantification of the length of mitochondria in sensory axons of 90 days old mitoDendra-TDP43^{A315T} mice. *n* (axons in 3 mice per group) = 17 mitoDendra and 22 mitoDendra-TDP43^{A315T}. n.s., non-significant. Error bars represent the SEM.

so far been largely limited to bioenergetics and molecular biology approaches.

Recent studies have addressed mitochondrial morphology or axonal transport *in vivo*, confirming that abnormalities are detectable in mutant SOD1 mice (10,19,20). Here, we sought to perform a broader analysis of neuronal mitochondrial changes, in young and adult mice, across different disease stages, in two distinct genetic models of FALS. We have investigated both transport and morphology of mitochondria at different axonal sites, from the axonal emergence (proximal segments) to the NMJ (distal segments). To our knowledge, this is the most extensive analysis of its kind, which has generated intriguing

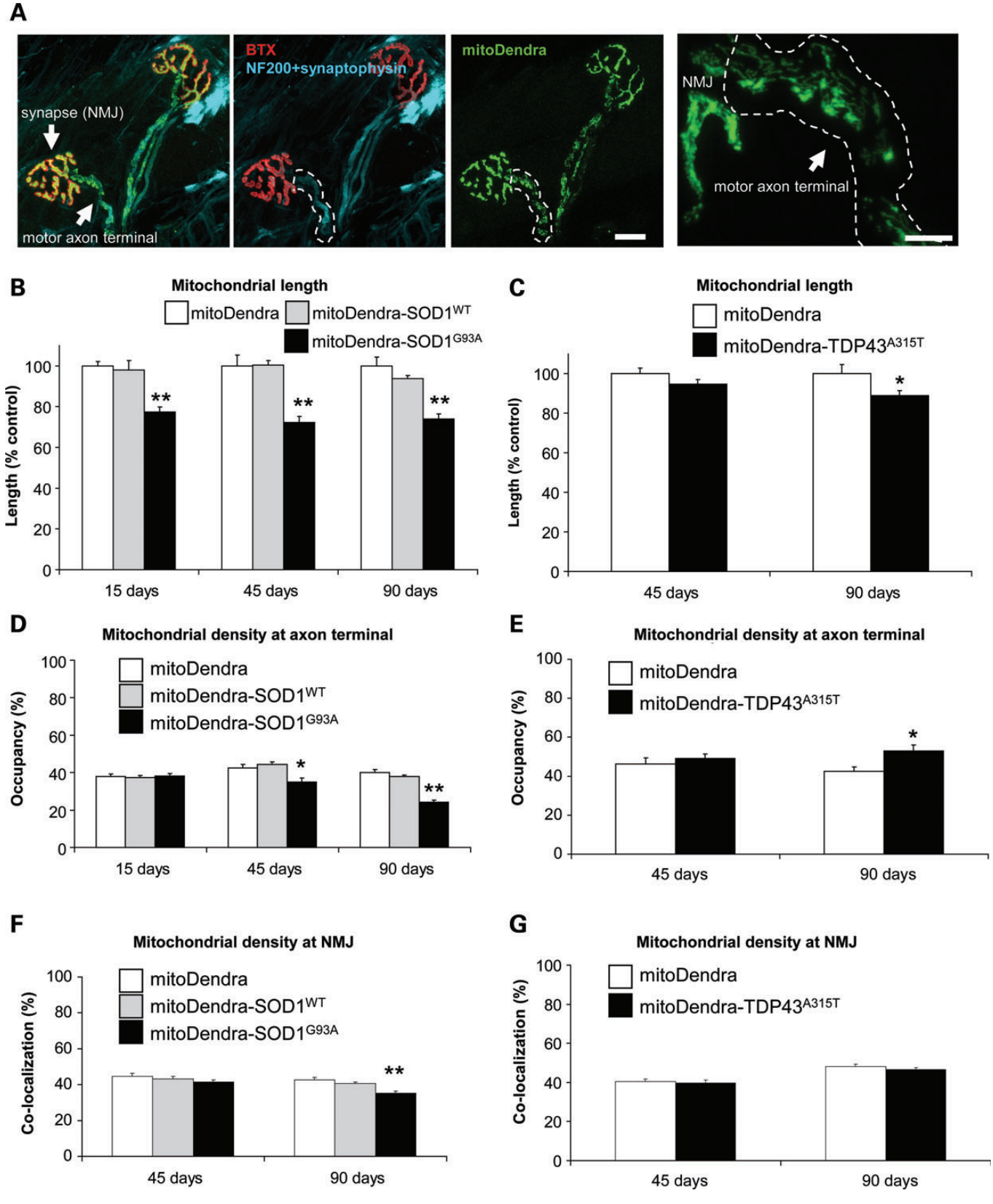
A
synapse (NMJ)
motor axon terminal
BTX
NF200+synaptophysin
mitoDendra
NMJ
motor axon terminal
B
Mitochondrial length
mitoDendra
mitoDendra-SOD1WT
mitoDendra-SOD1G93A
Length (% control)
15 days
45 days
90 days
C
Mitochondrial length
mitoDendra
mitoDendra-TDP43A315T
Length (% control)
45 days
90 days
D
Mitochondrial density at axon terminal
mitoDendra
mitoDendra-SOD1WT
mitoDendra-SOD1G93A
Occupancy (%)
15 days
45 days
90 days
E
Mitochondrial density at axon terminal
mitoDendra
mitoDendra-TDP43A315T
Occupancy (%)
45 days
90 days
F
Mitochondrial density at NMJ
mitoDendra
mitoDendra-SOD1WT
mitoDendra-SOD1G93A
Co-localization (%)
45 days
90 days
G
Mitochondrial density at NMJ
mitoDendra
mitoDendra-TDP43A315T
Co-localization (%)
45 days
90 days

observations. To investigate the transport and morphology of mitochondria *in vivo*, we have generated the mitoDendra mice, which can be also utilized in the future to study mitochondrial fusion, by taking advantage of the photo-conversion properties of mitoDendra (16,32). Our mitoDendra mouse differs from the recently described PhAM mouse because constitutive mitoDendra neuronal expression is achieved through the Thy1.2 promoter, instead of being conditionally expressed through Cre recombinase (33).

We have focused on pre-symptomatic disease stages in the genetic models of FALS to avoid the potential confounding effects of advanced neurodegeneration on the mitochondrial phenotype. Transport and morphological analyses were performed as early as 15 days of age. This was the earliest time that we could study, but still relevant to disease, since mitochondrial morphological abnormalities have been observed very early on in mutant SOD1 mice (9,34). The latest time point used for SOD1^{G93A} and TDP43^{A315T} mice (90 days of age) preceded the onset of overt motor impairment, although muscle denervation is known to occur at this age (25). Therefore, the study spanned different disease stages, but did not include the advanced symptomatic stages to avoid the extreme changes affecting terminally degenerated motor neurons.

It needs to be noted that the sciatic nerve is a convenient site for imaging mitochondrial transport in living mice, but it contains both motor and sensory axons. The Thy1.2 promoter used for the generation of the mitoDendra transgenic mouse does not allow for the distinction of the two types of neurons in the sciatic nerve. However, this genetic approach has the advantage of allowing the direct study of mitochondria from both motor and sensory neurons in the same mouse. When comparing mitochondrial morphology in other axonal segments, such as the roots and motor axon terminals (Figs 4 and 5), in both SOD1^{G93A} and TDP43^{A315T} mice, abnormal mitochondria were absent in sensory and motor roots, but were found in the motor axon terminals. These findings were in agreement with our observations *in vitro*, where mitochondrial abnormalities were only identified in distal segments of motor neurons (16).

A previous study of mitochondrial transport in the motor neuron axons of SOD1 transgenic mice evidenced abnormalities arising early on in the course of the disease (20). However, in that work, the results were interpreted as a lack of correlation between mitochondrial abnormalities and disease pathogenesis, because of two observations. First, transport abnormalities were found late in the life span of SOD1^{WT} mice. Here, we did not observe morphological or transport abnormalities in mitochondria from SOD1^{WT} mice at the time when SOD1^{G93A} mice presented overt defects. Nevertheless, it is known that overexpression of SOD1^{WT} can ultimately cause neurodegeneration and mitochondrial defects at advanced age, likely because SOD1^{WT} can also misfold and aggregate when expressed several folds above normal levels (35). Therefore, although SOD1^{WT} mice do not develop disease in their life span, they have CNS pathology.

Second, Marinkovic *et al*. (20) did not detect mitochondrial transport abnormalities in SOD1^{G85R} mice, until very late, a few days before the mice died. In both SOD1^{G93A} and TDP43^{A315T} mice, we detected transport alterations at early disease stages. We did not perform a time course study in the SOD1^{G85R} mice, because they have an atypical phenotype, whereby they are asymptomatic for a long time (10–12 months) and then develop massive protein aggregation in spinal cord neurons, muscle denervation and fatal paralysis within a few weeks.

Overall, we are convinced that the observations derived from our work and others' are consistent with a pathogenic role of mitochondrial transport abnormalities in neurons in SOD1 FALS mouse models.

In TDP43 mice, the occurrence of muscle denervation is not well characterized, although likely to occur at late time points (36). Denervation studies in TDP43^{A315T} mice have been difficult because these mice tend to die of ALS-unrelated causes, such as intestinal occlusion (23), before they have time to develop extensive muscle denervation. We observed a prominent clustering effect in the sciatic nerves of TDP43^{A315T} mice. Clustering has also been reported in the neuronal somas of TDP43^{WT} overexpressing mice (11,12). Furthermore, TDP43 overexpression in cultured motor neurons induced mitochondrial morphology and transport abnormalities (13).

Based on the observations from this study, it could be hypothesized that the sequence of pathological events in SOD1^{G93A} motor neurons involves early fragmentation of mitochondria in the sciatic nerve (Fig. 2B) and in distal segments of the motor axons (Fig. 5B), possibly caused by mitochondrial damage (37). These changes in mitochondrial morphology in motor terminals are to our knowledge the earliest abnormalities observed in SOD1^{G93A} motor neurons. They not only precede axonal degeneration and NMJ loss, but also activation of

Figure 5. Mitochondrial morphological abnormalities first appear in the motor terminals of mitoDendra-SOD1^{G93A} mice. (**A**) Representative image of the distal nerve segments of a motor neuron in the trapezius muscle of a 45 days old mitoDendra-SOD1^{WT} mouse. Axons were labeled with NF200 and synaptophysin (in blue), and NMJs identified by fluorescent α-bungarotoxin (BTX, in red). The masks of the axonal labeling (dotted area) and NMJ area were obtained in an unbiased manner, and used to determine the occupancy of mitochondria in the motor axon terminal and synapse, respectively. Scale bar, 20 μm. Detail of mitochondria in the motor terminal; note the tightly packed mitochondria network in the NMJ. Scale bar, 5 μm. (**B**) Quantification of the length of mitochondria in the nerve terminals during disease progression. Values are expressed as mean percentage ± SEM of mitoDendra controls. *n* (axons at 15–45–90 days in 3 mice per group) = 34–8–14 mitoDendra, 19–20–11 mitoDendra-SOD1^{WT}, 28–29–14 mitoDendra-SOD1^{G93A}. (**C**) Mitochondrial morphology abnormalities are observed in the nerve terminals of mitoDendra-TDP43^{A315T} mice at later stages. Quantification of the length of mitochondria in the nerve terminals of mitoDendra-TDP43 mice. *n* (axons at 45–90 days in 3–4 mice per group) = 21–20 mitoDendra, 30–22 mitoDendra-TDP43^{A315T}. (**D**) Quantification of mitochondrial density at motor terminals of mitoDendra-SOD1 mice defined by the occupancy of mitochondria within axon terminals (% of thresholded area). *n* (axons at 15–45–90 days in 3 mice per group) = 35–21–35 mitoDendra, 34–39–19 mitoDendra-SOD1^{WT}, 33–55–59 mitoDendra-SOD1^{G93A}. (**E**) Abnormal accumulation of mitochondria in the axon terminals of mitoDendra-TDP43^{A315T} mice. Quantification of the mitochondrial density in the nerve terminals of mitoDendra-TDP43 mice. *n* (NMJs at 45–90 days in 3–4 mice per group) = 9–11 mitoDendra, 24–21 mitoDendra-TDP43^{A315T}. (**F**) Quantification of the mitochondrial density at the NMJs in mitoDendra-SOD1 mice. Data are presented as percentage of co-localization of NMJ area (red fluorescence) over mitochondria (green fluorescence). *n* (NMJs at 45–90 days in 3 mice per group) = 37–42 mitoDendra, 49–50 mitoDendra-SOD1^{WT} and 70–65 mitoDendra-SOD1^{G93A}. (**G**) No accumulation of mitochondria at the NMJs of mitoDendra-TDP43^{A315T} mice. Quantification of the mitochondrial density in the NMJ of mitoDendra-TDP43 mice. *n* (NMJs at 45–90 days in 3–4 mice per group) = 25–42 mitoDendra, 44–30 mitoDendra-TDP43^{A315T}. $^{*}P < 0.05$ and $^{**}P < 0.01$ by Student's *t*-test, versus mitoDendra controls. Error bars represent the SEM.

astrocytes and microglia in the spinal cord. Although non-cell autonomous effects on motor neuron mitochondria cannot be completely excluded, even in the absence of glial activation, our findings suggest that early mitochondrial abnormalities in motor neurons could be a trigger rather than a target of the degenerative process in SOD1^{G93A} mice. Thus, mitochondrial abnormalities may activate quality control degradation pathways in distal regions, which could explain the distal depletion of mitochondria (Fig. 5D and F) and the alteration of mitochondrial axonal transport (Fig. 1B) at later stages of the disease. The impairment of mitochondrial distribution to synapses may result in energy deprivation and failure to buffer Ca^{2+} in response to neuronal depolarization around synaptic regions, and therefore may contribute to the early denervation process (38) due to bioenergetic failure at the synapse.

Altered mitochondrial transport, which initially affects retrograde moving mitochondria and later also affects anterograde movement (Fig. 1C and D), may also contribute to the fragmentation and abnormal distribution of mitochondria along motor axons and in the NMJs when SOD1^{G93A} mice approached the symptomatic disease stage (Figs 2 and 5). Indeed, perturbations in retrograde axonal transport result in progressive motor neuron degeneration *in vivo* (39). Axonal mitochondrial clusters (Fig. 2F), which had also been found *in vivo* using immunocytochemistry (30), may follow altered axonal transport.

In TDP43^{A315T} mice, on the other hand, the earliest mitochondrial defect we could detect was not fragmentation but reduced retrograde axonal transport (Fig. 1E). It is currently unknown whether TDP43^{A315T} causes alterations on mitochondrial bioenergetics, a question that needs further analysis. Early defects in mitochondrial retrograde transport may be responsible for an imbalance in mitochondrial distribution along the motor axons, such as the accumulation of mitochondria in the motor axon terminals because of defective mobilization of mitochondria (Fig. 5E), and mitochondrial fragmentation (Figs 2C and 5C). The observed accumulation of mitochondria near the NMJs of TDP43^{A315T} mice differs from what was previously described in TDP43^{WT} mice, where mitochondria were depleted (12); this conflicting data points to potential differences in the mitochondrial transport mechanisms in the two TDP43 transgenic models. Finally, defects in anterograde-moving mitochondria at later stages (Fig. 1F) may also contribute to the overall defects on mitochondria morphology and distribution (Figs 2 and 5).

Since both mutant SOD1 (40) and TDP43 (13) have been found in association with the mitochondrial outer membrane, it is plausible that they may interfere with the proper interactions between mitochondria and the axonal transport machinery. Mitochondrial retrograde transport was affected earlier than anterograde transport in both SOD1^{G93A} and TDP43^{A315T} mice (Fig. 1), suggesting that these mutant proteins may interact with the retrograde transport machinery directly, as shown in mutant SOD1 mice (41), although such potential interactions have not been investigated in TDP43 mice.

In conclusion, these studies provide a first comparative *in vivo* analysis of mitochondrial dynamics, morphology and distribution in the nervous system of mice expressing mutant SOD1 and TDP43. A new mitoDendra mouse was used to image mitochondria in intact peripheral nerves of living mice. The results shown here demonstrate that mitochondrial transport abnormalities are a common denominator in the two different genetic models of FALS. Similarities are recorded in the transport defects and the morphological and distribution changes. However, differences among the genetic forms are also evident, especially regarding the spatio-temporal pattern of appearance, suggesting that different molecular mechanisms may be involved. Although further studies will be needed to better understand these mechanisms, the early onset of mitochondrial abnormalities *in vivo* suggests that they are involved in the pathogenic process, especially in distal segments of the axons and the NMJ, which are primary disease targets in ALS.

MATERIALS AND METHODS

Generation of Thy1.2-mitoDendra transgenic mice

MitoDendra cDNA (16) was cloned into the *Sal*I-*Xho*I sites of the *Thy1.2* promoter (a kind gift from Dr Frank LaFerla). The transgene was injected into fertilized hybrid B6SJLF1 eggs at the Weill Medical College Transgenic Core facilities. Screening of the transgenic founders was performed by Southern blot analysis of tail DNA and confirmed by PCR. Ten identified genetically positive founders (named TM, followed by the founder number) were subsequently bred with B6SJLF1/J mice (The Jackson Laboratory). All studies in this work were performed using mitoDendra line TM57.

FALS mouse models

We used the strains B6SJL-Tg(SOD1*G93A)1Gur/J, B6SJL-Tg(SOD1)2Gur/J and B6;CB-Tg(Prnp-TARDBP*A315T) 95Balo/J for SOD1^{G93A}, SOD1^{WT} and TDP43^{A315T} transgenic mice, respectively (all three strains were from The Jackson Laboratory). TDP43^{A315T} mice originally obtained were in a mixed background. Therefore, they were brought to a congenic B6SJLF1 genetic background by backcrossing them with B6SJLF1 breeders. SOD1 and TDP43 males were bred to mitoDendra female mice. The resulting double transgenic mice mitoDendra-SOD1^{WT}, mitoDendra-SOD1^{G93A}, mitoDendra-TDP43^{A315T} and corresponding mitoDendra non-SOD1 and non-TDP43 littermates were identified by genotyping using PCR analyses of tail DNA. All experiments were approved by the Weill Cornell Medical College Institutional Animal Care and Use Committee. Principles of laboratory animal care (NIH publication No. 86-23, revised 1985) were followed, as well as specific national laws (e.g. the current version of the German Law on the Protection of Animals), where applicable.

The criterion for determining disease onset was the development of abnormal hind-limb extension (clasping). The criterion for survival was the inability of the mouse to right itself, when placed on its side (loss of righting reflex).

In vivo live-imaging

Mice were anesthetized with ketamine (87 mg/kg IP) and xylazine (13 mg/kg IP) and immobilized onto a platform. With the help of a binocular dissecting microscope, a small surgical incision was made in the thigh to expose the sciatic nerve. Caution was taken to avoid any bleeding or damaging of the surrounding tissue. The surgical cavity was filled with artificial CSF solution

(in mM: NaCl 117, KCl 4.7, $CaCl_2$ 2.5, $MgCl_2$ 1.2, $NaHCO_3$ 25, NaH_2PO_4 1.2 and glucose 11 at pH 7.4).

Images of mitoDendra fluorescent mitochondria were taken with a Bio-Rad Radiance 2000 confocal microscope, using 1.5 mW 488-nm laser intensity, a 60× water immersion objective (N.A. 1.0; with 2× zoom) and a pinhole of 5.4 AU. Stacks of four z-sections were taken at 1.5 μm intervals, every 5 s, for 6 min. Images were 8-bit color.

Analysis of mitochondrial transport

Mitochondrial transport was analyzed in movies that resulted from merged z-sections (using best focus projection) after a low pass filter was applied. The total number of mitochondria was counted for each axonal segment in a given field. Mitochondria were defined as mobile if they changed their position in at least three consecutive frames (16). For each analyzed axon, the number of mobile mitochondria was assessed for the entire duration of the movie (6 min) and data were plotted as a percentage of the total number of mitochondria. Directions of transport were referred to as anterograde or retrograde to describe mitochondria moving toward the motor axon terminals or the spinal cord, respectively.

Tissue processing and staining

For immunohistochemistry analyses, deeply anesthetized mice were perfused transcardially with ice-cold PBS followed by 4% paraformaldehyde in PBS. Spinal cord, sciatic nerves and trapezius muscles were harvested. Nervous tissues were cryoprotected in 30% sucrose, and muscles were stored in PBS at 4°C. Cryosections were obtained from the lumbar region of the spinal cord (20 μm thick) and the sciatic nerves (10 μm thick).

Muscles were stained with standard immunohistochemistry protocols to label motor axons, using antibodies against neurofilament 200 (NF200, Sigma) and synaptophysin (Chemicon). Briefly, muscles were incubated in blocking buffer (5% NGS, 2.5% BSA, 1% Triton X-100 in PBS) overnight, followed by a second incubation with primary antibodies (in blocking buffer). Specimens were then washed in PBS for 12 h, and then incubated with secondary fluorescent antibodies (in blocking buffer), overnight. All steps were carried out at 4°C. Cy5-conjugated secondary antibodies (Jackson ImmunoResearch) were used. Post-synaptic acetylcholine receptors were detected with tetramethylrhodamine-labeled α-bungarotoxin (BTX; Invitrogen).

Mitochondrial morphology and density analysis

Images from fixed specimens were collected in a Leica TCS SP5 Confocal Microscope (Leica Microsystems), using the following lenses for various applications: a 10× dry, a 40× oil and a 63× oil immersion, with NA 0.30, 1.25 and 1.4, respectively. A standard pinhole of 1 AU and optical intervals of 1 μm (4 μm for 10× lens) were used. When required, a 5× zoom was applied and optical intervals of 0.5 μm used. For each tissue analyzed (sciatic, spinal cord, muscle), at least three fields containing several axons were imaged randomly. Metamorph software (Universal Imaging) was used for quantitative analysis of mitochondrial morphology measurements, as previously described (15). Mitochondrial clustering was defined as the accumulation of several mitoDendra-labeled mitochondria, which could be distinguished as being individual mitochondrial units, but assembled in irregularly shaped structures (not tubular) of more than 2 μm thick and 5 μm long (15). Distribution of clusters was expressed as the number of clusters per 50 μm of axonal segments.

For quantitative analysis of mitochondrial density at nerve terminals and NMJs, z-sections were merged (using maximal projection) and the threshold was set to at least twice the background fluorescence. The density of mitochondria at the nerve terminal was measured by the occupancy (% of thresholded area) of mitochondria within a 30–100 μm long axonal segment (identified by immunolabeling with synaptophysin and NF200 antibodies). For the analysis at the NMJs, mitochondrial density was measured by the percentage of the area of NMJ (defined by postsynaptic labeling with fluorescent BTX) overlapping green fluorescent mitochondria (% of co-localization of red over green fluorescence).

Statistical analysis

Statistical comparisons of mitoDendra-FALS with mitoDendra littermate controls were made by Student's two-tailed, unpaired *t*-test. A *P*-value of <0.05 was considered significant. Results were expressed as the mean ± SE. The number of samples corresponds to the number of studied axons or NMJs, from three or more mice per each genotype and at each time point.

SUPPLEMENTARY MATERIAL

Supplementary Material is available at *HMG* online.

ACKNOWLEDGEMENTS

We thank Dr Frank LaFerla (University of California) for providing the Thy1.2 promoter.

FUNDING

This work was supported by the Robert Packard Center for ALS Research 'The New York Community Trust' to J.M. and G.M.; the Muscular Dystrophy Association to J.M.; and the National Institutes of Health NS047325 (to W.-B.G.), NS051419 and NS062055 (to G.M.).

REFERENCES

1. Faes, L. and Callewaert, G. (2011) Mitochondrial dysfunction in familial amyotrophic lateral sclerosis. *J. Bioenerg. Biomembr.*, **43**, 587–592.
2. Cozzolino, M., Ferri, A., Valle, C. and Carri, M.T. (2013) Mitochondria and ALS: implications from novel genes and pathways. *Mol. Cell. Neurosci.*, **55**, 44–49.
3. Gurney, M.E., Pu, H., Chiu, A.Y., Dal Canto, M.C., Polchow, C.Y., Alexander, D.D., Caliendo, J., Hentati, A., Kwon, Y.W., Deng, H.X. *et al.* (1994) Motor neuron degeneration in mice that express a human Cu,Zn superoxide dismutase mutation [see comments] [published erratum appears in Science 1995 Jul 14;269(5221):149]. *Science*, **264**, 1772–1775.
4. Wong, P.C., Pardo, C.A., Borchelt, D.R., Lee, M.K., Copeland, N.G., Jenkins, N.A., Sisodia, S.S., Cleveland, D.W. and Price, D.L. (1995) An adverse property of a familial ALS-linked SOD1 mutation causes motor

neuron disease characterized by vacuolar degeneration of mitochondria. *Neuron*, **14**, 1105–1116.
5. Kong, J. and Xu, Z. (1998) Massive mitochondrial degeneration in motor neurons triggers the onset of amyotrophic lateral sclerosis in mice expressing a mutant SOD1. *J. Neurosci.*, **18**, 3241–3250.
6. Mattiazzi, M., D'Aurelio, M., Gajewski, C.D., Martushova, K., Kiaei, M., Beal, M.F. and Manfredi, G. (2002) Mutated human SOD1 causes dysfunction of oxidative phosphorylation in mitochondria of transgenic mice. *J. Biol. Chem.*, **277**, 29626–29633.
7. Vande Velde, C., Garcia, M.L., Yin, X., Trapp, B.D. and Cleveland, D.W. (2004) The neuroprotective factor Wlds does not attenuate mutant SOD1-mediated motor neuron disease. *Neuromol. Med.*, **5**, 193–203.
8. Damiano, M., Starkov, A.A., Petri, S., Kipiani, K., Kiaei, M., Mattiazzi, M., Flint Beal, M. and Manfredi, G. (2006) Neural mitochondrial Ca2+ capacity impairment precedes the onset of motor symptoms in G93A Cu/Zn-superoxide dismutase mutant mice. *J. Neurochem.*, **96**, 1349–1361.
9. Gould, T.W., Buss, R.R., Vinsant, S., Prevette, D., Sun, W., Knudson, C.M., Milligan, C.E. and Oppenheim, R.W. (2006) Complete dissociation of motor neuron death from motor dysfunction by Bax deletion in a mouse model of ALS. *J. Neurosci.*, **26**, 8774–8786.
10. Vande Velde, C., McDonald, K.K., Boukhedimi, Y., McAlonis-Downes, M., Lobsiger, C.S., Bel Hadj, S., Zandona, A., Julien, J.P., Shah, S.B. and Cleveland, D.W. (2011) Misfolded SOD1 associated with motor neuron mitochondria alters mitochondrial shape and distribution prior to clinical onset. *PLoS ONE*, **6**, e22031.
11. Xu, Y.F., Gendron, T.F., Zhang, Y.J., Lin, W.L., D'Alton, S., Sheng, H., Casey, M.C., Tong, J., Knight, J., Yu, X. *et al.* (2010) Wild-type human TDP-43 expression causes TDP-43 phosphorylation, mitochondrial aggregation, motor deficits, and early mortality in transgenic mice. *J. Neurosci.*, **30**, 10851–10859.
12. Shan, X., Chiang, P.M., Price, D.L. and Wong, P.C. (2010) Altered distributions of Gemini of coiled bodies and mitochondria in motor neurons of TDP-43 transgenic mice. *Proc. Natl Acad. Sci. USA*, **107**, 16325–16330.
13. Wang, W., Li, L., Lin, W.L., Dickson, D.W., Petrucelli, L., Zhang, T. and Wang, X. (2013) The ALS disease-associated mutant TDP-43 impairs mitochondrial dynamics and function in motor neurons. *Hum. Mol. Genet.*, **22**, 4706–4719.
14. De Vos, K.J., Chapman, A.L., Tennant, M.E., Manser, C., Tudor, E.L., Lau, K.F., Brownlees, J., Ackerley, S., Shaw, P.J., McLoughlin, D.M. *et al.* (2007) Familial amyotrophic lateral sclerosis-linked SOD1 mutants perturb fast axonal transport to reduce axonal mitochondria content. *Hum. Mol. Genet.*, **16**, 2720–2728.
15. Magrane, J., Hervias, I., Henning, M.S., Damiano, M., Kawamata, H. and Manfredi, G. (2009) Mutant SOD1 in neuronal mitochondria causes toxicity and mitochondrial dynamics abnormalities. *Hum. Mol. Genet.*, **18**, 4552–4564.
16. Magrane, J., Sahawneh, M.A., Przedborski, S., Estevez, A.G. and Manfredi, G. (2012) Mitochondrial dynamics and bioenergetic dysfunction is associated with synaptic alterations in mutant SOD1 motor neurons. *J. Neurosci.*, **32**, 229–242.
17. Song, W., Song, Y., Kincaid, B., Bossy, B. and Bossy-Wetzel, E. (2013) Mutant SOD1G93A triggers mitochondrial fragmentation in spinal cord motor neurons: neuroprotection by SIRT3 and PGC-1alpha. *Neurobiol. Dis.*, **51**, 72–81.
18. Ilieva, H., Polymenidou, M. and Cleveland, D.W. (2009) Non-cell autonomous toxicity in neurodegenerative disorders: ALS and beyond. *J. Cell Biol.*, **187**, 761–772.
19. Bilsland, L.G., Sahai, E., Kelly, G., Golding, M., Greensmith, L. and Schiavo, G. (2010) Deficits in axonal transport precede ALS symptoms in vivo. *Proc. Natl Acad. Sci. USA*, **107**, 20523–20528.
20. Marinkovic, P., Reuter, M.S., Brill, M.S., Godinho, L., Kerschensteiner, M. and Misgeld, T. (2012) Axonal transport deficits and degeneration can evolve independently in mouse models of amyotrophic lateral sclerosis. *Proc. Natl Acad. Sci. USA*, **109**, 4296–4301.
21. Caroni, P. (1997) Overexpression of growth-associated proteins in the neurons of adult transgenic mice. *J. Neurosci. Methods*, **71**, 3–9.
22. Wegorzewska, I., Bell, S., Cairns, N.J., Miller, T.M. and Baloh, R.H. (2009) TDP-43 mutant transgenic mice develop features of ALS and frontotemporal lobar degeneration. *Proc. Natl Acad. Sci. USA*, **106**, 18809–18814.
23. Esmaeili, M.A., Panahi, M., Yadav, S., Hennings, L. and Kiaei, M. (2013) Premature death of TDP-43 (A315T) transgenic mice due to gastrointestinal complications prior to development of full neurological symptoms of amyotrophic lateral sclerosis. *Int. J. Exp. Pathol.*, **94**, 56–64.
24. Misgeld, T., Kerschensteiner, M., Bareyre, F.M., Burgess, R.W. and Lichtman, J.W. (2007) Imaging axonal transport of mitochondria in vivo. *Nat. Methods*, **4**, 559–561.
25. Fischer, L.R., Culver, D.G., Tennant, P., Davis, A.A., Wang, M., Castellano-Sanchez, A., Khan, J., Polak, M.A. and Glass, J.D. (2004) Amyotrophic lateral sclerosis is a distal axonopathy: evidence in mice and man. *Exp. Neurol.*, **185**, 232–240.
26. Pun, S., Santos, A.F., Saxena, S., Xu, L. and Caroni, P. (2006) Selective vulnerability and pruning of phasic motoneuron axons in motoneuron disease alleviated by CNTF. *Nat. Neurosci.*, **9**, 408–419.
27. Schaefer, A.M., Sanes, J.R. and Lichtman, J.W. (2005) A compensatory subpopulation of motor neurons in a mouse model of amyotrophic lateral sclerosis. *J. Comp. Neurol.*, **490**, 209–219.
28. Valdez, G., Tapia, J.C., Lichtman, J.W., Fox, M.A. and Sanes, J.R. (2012) Shared resistance to aging and ALS in neuromuscular junctions of specific muscles. *PLoS ONE*, **7**, e34640.
29. Nagai, M., Re, D.B., Nagata, T., Chalazonitis, A., Jessell, T.M., Wichterle, H. and Przedborski, S. (2007) Astrocytes expressing ALS-linked mutated SOD1 release factors selectively toxic to motor neurons. *Nat. Neurosci.*, **10**, 615–622.
30. Sotelo-Silveira, J.R., Lepanto, P., Elizondo, V., Horjales, S., Palacios, F., Martinez-Palma, L., Marin, M., Beckman, J.S. and Barbeito, L. (2009) Axonal mitochondrial clusters containing mutant SOD1 in transgenic models of ALS. *Antioxid. Redox Signal*, **11**, 1535–1545.
31. Ohno, N., Kidd, G.J., Mahad, D., Kiryu-Seo, S., Avishai, A., Komuro, H. and Trapp, B.D. (2011) Myelination and axonal electrical activity modulate the distribution and motility of mitochondria at CNS nodes of Ranvier. *J. Neurosci.*, **31**, 7249–7258.
32. Gurskaya, N.G., Verkhusha, V.V., Shcheglov, A.S., Staroverov, D.B., Chepurnykh, T.V., Fradkov, A.F., Lukyanov, S. and Lukyanov, K.A. (2006) Engineering of a monomeric green-to-red photoactivatable fluorescent protein induced by blue light. *Nat. Biotechnol.*, **24**, 461–465.
33. Pham, A.H., McCaffery, J.M. and Chan, D.C. (2012) Mouse lines with photo-activatable mitochondria to study mitochondrial dynamics. *Genesis*, **50**, 833–843.
34. Bendotti, C., Calvaresi, N., Chiveri, L., Prelle, A., Moggio, M., Braga, M., Silani, V. and De Biasi, S. (2001) Early vacuolization and mitochondrial damage in motor neurons of FALS mice are not associated with apoptosis or with changes in cytochrome oxidase histochemical reactivity. *J. Neurol. Sci.*, **191**, 25–33.
35. Jaarsma, D., Rognoni, F., van Duijn, W., Verspaget, H.W., Haasdijk, E.D. and Holstege, J.C. (2001) Cuzn superoxide dismutase (SOD1) accumulates in vacuolated mitochondria in transgenic mice expressing amyotrophic lateral sclerosis-linked SOD1 mutations. *Acta Neuropathol. (Berl.)*, **102**, 293–305.
36. Zhou, H., Huang, C., Chen, H., Wang, D., Landel, C.P., Xia, P.Y., Bowser, R., Liu, Y.J. and Xia, X.G. (2010) Transgenic rat model of neurodegeneration caused by mutation in the TDP gene. *PLoS Genet.*, **6**, e1000887.
37. Kawamata, H. and Manfredi, G. (2010) Mitochondrial dysfunction and intracellular calcium dysregulation in ALS. *Mech. Ageing Dev.*, **131**, 517–526.
38. Martin, L.J. (2011) Mitochondrial pathobiology in ALS. *J. Bioenerg. Biomembr.*, **43**, 569–579.
39. Hafezparast, M., Klocke, R., Ruhrberg, C., Marquardt, A., Ahmad-Annuar, A., Bowen, S., Lalli, G., Witherden, A.S., Hummerich, H., Nicholson, S. *et al.* (2003) Mutations in dynein link motor neuron degeneration to defects in retrograde transport. *Science*, **300**, 808–812.
40. Vande Velde, C., Miller, T.M., Cashman, N.R. and Cleveland, D.W. (2008) Selective association of misfolded ALS-linked mutant SOD1 with the cytoplasmic face of mitochondria. *Proc. Natl Acad. Sci. USA*, **105**, 4022–4027.
41. Strom, A.L., Gal, J., Shi, P., Kasarskis, E.J., Hayward, L.J. and Zhu, H. (2008) Retrograde axonal transport and motor neuron disease. *J. Neurochem.*, **106**, 495–505.